Magnetic Order and Dynamics in an Orbitally Degenerate Ferromagnetic Insulator

C. Ulrich,[1] G. Khaliullin,[1] S. Okamoto,[1,2] M. Reehuis,[3] A. Ivanov,[4] H. He,[1] Y. Taguchi,[5] Y. Tokura,[5] and B. Keimer[1]

[1]*Max-Planck-Institut für Festkörperforschung, 70569 Stuttgart, Germany*
[2]*Institute of Physical and Chemical Research (RIKEN), Saitama 351-0198, Japan*
[3]*Hahn-Meitner-Institut, 14109 Berlin, Germany*
[4]*Institut Laue-Langevin, 156X, 38042 Grenoble, France*
[5]*Department of Applied Physics, University of Tokyo, 113 Tokyo, Japan*

(Received 8 April 2002; published 25 September 2002)

Neutron scattering was used to determine the spin structure and the magnon spectrum of the Mott-Hubbard insulator $YTiO_3$. The magnetic structure is complex, comprising substantial *G*-type and *A*-type antiferromagnetic components in addition to the predominant ferromagnetic component. The magnon spectrum, on the other hand, is gapless and nearly isotropic. We show that these findings are inconsistent with the orbitally ordered states thus far proposed for $YTiO_3$ and discuss general implications for a theoretical description of exchange interactions in orbitally degenerate systems.

DOI: 10.1103/PhysRevLett.89.167202 PACS numbers: 75.30.Et, 75.30.Ds, 75.30.Gw, 75.50.Ee

The interplay between spin and orbital degrees of freedom in transition metal oxides has been a subject of investigation since the 1950s. As one of the salient outcomes of this effort, the "Goodenough-Kanamori rules" provide a description of the exchange interactions between magnetic atoms and, hence, the magnetic ordering pattern, in terms of the relative orientation of valence orbitals on neighboring lattice sites. This field has recently moved back into the center of attention [1], as advances in materials preparation have made it possible to investigate not only the *static* spin and orbital arrangements, but also the spin and orbital *dynamics* in *d*-electron systems. In cubic manganites, the focus of much of the recent attention, the spin wave excitations have been studied extensively [2], and excitations associated with the *d*-orbital degrees of freedom have recently also been detected [3].

The cubic crystal field in the perovskite structure splits the degenerate *d*-orbital manifold of a free transition metal ion into a lower-lying triplet of t_{2g} symmetry and a higher-lying e_g doublet. In the manganites, where the e_g doublet is partially occupied, coupling to the lattice through the Jahn-Teller effect lifts the orbital degeneracy and generally pushes the orbital excitations to energies much larger than the magnon bandwidth. The spin and orbital dynamics are thus largely decoupled, and quantum effects are suppressed. For t_{2g} orbitals, on the other hand, the higher degeneracy and the more isotropic, less bond-directional charge distribution reduces the lattice coupling, and one may expect a more dramatic interplay between the orbital and the spin dynamics. The manifestations of this interplay should be most apparent for a single *d* electron in the t_{2g} manifold, a situation realized in the pseudocubic titanates. Indeed, the magnetic properties of the Mott-Hubbard insulator $LaTiO_3$ are difficult to reconcile with predictions based on the standard Goodenough-Kanamori rules. The *G*-type antiferromagnetic ground state [4] of $LaTiO_3$ is in conflict with the predictions of all electronic structure calculations thus far reported [5,6]. Further, its ordered moment is smaller and its spin wave spectrum is more isotropic than predicted by conventional superexchange models [7].

The theoretical implications of the unusual magnetic properties of $LaTiO_3$ have remained controversial. The theories thus far proposed invoke disparate effects ranging from a subtle, hitherto unobserved lattice distortion [8] to a novel spin-orbital resonance [9,10]. We have investigated the microscopic magnetic properties of $YTiO_3$, a sister compound of $LaTiO_3$ whose larger O-Ti-O bond distortion results in a reduced electronic bandwidth and an increased Mott-Hubbard gap [11,12]. In contrast to $LaTiO_3$, the ferromagnetic ground state of $YTiO_3$ (Ref. [13]) is in accord with electronic structure calculations [5,6]. However, our inelastic neutron scattering study reveals a magnon spectrum that cannot be explained in terms of the orbital ordering patterns thus far proposed. We discuss our results in light of current theories of superexchange in the presence of orbital degeneracy.

The sample was an untwinned single crystal of volume 0.4 cm^3 grown by the floating zone technique as described elsewhere [11]. The neutron scattering experiments were performed at the IN22 triple-axis spectrometer at the Institut Laue-Langevin in Grenoble, France, and at the E5 four-circle diffractometer at the BER-II reactor of the Hahn-Meitner Institute in Berlin, Germany. For the measurements on IN22, a pyrolytic graphite (PG) monochromator and a PG-analyzer, both horizontally collimating, were used. Depending on kinematic constraints and resolution requirements, the final wave vector was fixed at 1.64, 2.66, or 4.10 $Å^{-1}$. On E5, neutron wavelengths 2.36 or 0.902 Å were selected by a PG or a Cu monochromator, respectively, and the data were collected with a two-dimensional position sensitive ^{3}He detector.

A set of 1359 structural Bragg reflections taken on E5 [14] could be refined with the orthorhombic space group

 © 2002 The American Physical Society

Pnma and room temperature lattice parameters $a = 5.3584(9)$ Å, $b = 5.6956(8)$ Å, and $c = 7.6371(11)$ Å, in agreement with previous reports [4,15]. In order to simplify the comparison to model calculations, we sometimes use the pseudocubic (c) unit cell with lattice parameters $a' = a/\sqrt{2}$, $b' = b/\sqrt{2}$, and $c' = c/2$ instead of the full orthorhombic (o) cell. Our data provide no indication of a structural phase transition below room temperature.

The presence of magnetic intensity could be established from the temperature dependence of the primitive Bragg reflections at low momentum transfer, some of which show a spontaneous increase in intensity below $T_C = 27$ K (Fig. 1). The reflections $(2,0,0)_o$, $(0,2,0)_o$, $(1,1,0)_o$, and $(1,1,2)_o$ show the strongest magnetic intensities, indicating a predominantly ferromagnetic coupling of the Ti moments as previously reported [4]. In addition, however, magnetic Bragg reflections were also observed at $(0,1,1)_o$, $(1,0,1)_o$, $(0,0,1)_o$, and $(0,0,3)_o$ [Fig. 1(b)]. This indicates the presence of hitherto unobserved staggered components of the ordered moment. A full analysis of the magnetic diffraction pattern at $T = 10$ K gives the following components of the ordered moment per Ti^{3+} ion: a ferromagnetic component of $0.544(11)\mu_B$ along c; a G-type antiferromagnetic component of $0.082(12)\mu_B$ along a; and an A-type antiferromagnetic component of $0.047(13)\mu_B$ along b. In agreement with Bertaut's representation analysis [16], the magnetic structure can thus be described by the basis functions G_x, A_y, and F_z [17]. A pictorial representation is given in the inset in Fig. 1. The total magnetic moment at 10 K is $0.553(11)\mu_B/Ti^{3+}$-ion. Since the magnetic Bragg peak intensity is not saturated at 10 K, this extrapolates to $0.715\mu_B$ at $T = 0$, somewhat lower than the saturated moment of $0.84\mu_B$ previously reported for samples with proportionally higher Curie temperatures [19].

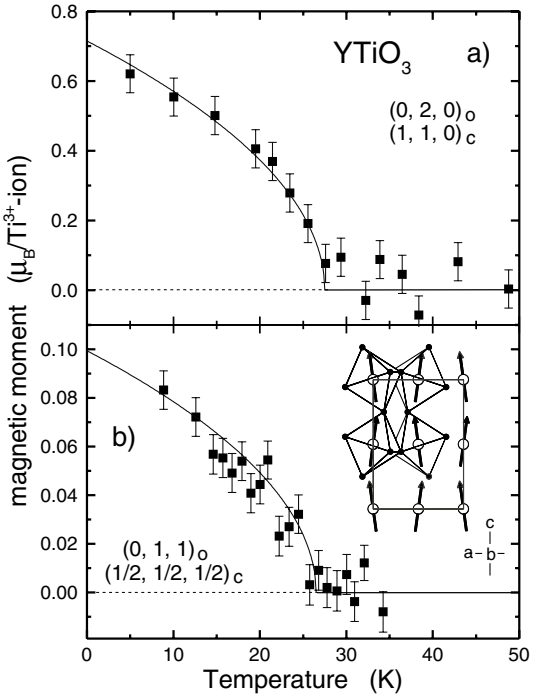

FIG. 1. (a) Ferromagnetic and (b) G-type antiferromagnetic components of the ordered magnetic moment of $YTiO_3$ extracted from the amplitudes of the $(0,2,0)_o$ and $(0,1,1)_o$ magnetic Bragg reflections, respectively. A weakly temperature dependent nuclear contribution to both reflections has been subtracted. The inset gives a pictorial representation of the magnetic structure. The TiO_6 octahedra are highlighted.

We now turn to the determination of the spin wave spectrum by inelastic neutron scattering. Figure 2 shows representative constant-$\mathbf{q}$ scans at $T = 5$ and 50 K, that is, above and below T_C. As shown in the figure, magnons can be distinguished from phonons on the basis of their temperature dependence. While the former become overdamped above T_C, the latter only show a slight intensity change due to the thermal population factor. Since the line shape of the observed features is strongly influenced by the spectrometer resolution, a deconvolution is required to accurately extract the spin wave peak positions. We have used both the standard Cooper-Nathans procedure and a Monte Carlo ray-tracing routine [20]. Some of the resulting profiles are shown in Fig. 2.

The inelastic neutron scattering data are summarized in Fig. 3. Some features of the spectrum are immediately apparent. First, the spectrum is gapless: by high resolution constant-$\mathbf{q}$ scans at the zone center we have obtained an upper bound of 0.3 meV on the spin wave gap. Second, the spectrum is almost isotropic: a surprisingly good fit can be obtained by an isotropic Heisenberg model which gives a dispersion of the form $\hbar\omega = 6S|J|(1 - \gamma_{\mathbf{q}})$ with $\gamma_{\mathbf{q}} = \frac{1}{3}[\cos(q_x a') + \cos(q_y b') + \cos(q_z c')]$ and $S = 1/2$. The best fit of the spectrum is obtained by a nearest-neighbor superexchange parameter $J = -3.0$ meV, corresponding [21] to $T_C = [1.45S(S+1) - 0.18]|J|/k_B = 32$ K, which agrees well with the experimental value. A small systematic deviation from the result of this fit is noticeable, albeit within the experimental error bars (Fig. 3). The fit can be improved by introducing either a subtle ($\sim 6\%$) difference between the exchange parameters in the ab plane and along the c axis, or by incorporating a small exchange anisotropy that is also required to explain the noncollinear spin structure. Specifically, the leading anisotropy term in the spin Hamiltonian of the titanates is of cubic symmetry [10] and modifies the magnon dispersion as follows:

$$\hbar\omega = \sqrt{3|J|(1 - \gamma_{\mathbf{q}}) + \Delta + A[1 - \cos(q_x a')]} \times \sqrt{3|J|(1 - \gamma_{\mathbf{q}}) + \Delta + A[1 - \cos(q_y b')]}, \quad (1)$$

where A is the anisotropy parameter and $\Delta = 0.093A^2/|J|$ is the spin wave gap. The best fit gives $A = 0.8$ meV and $J = -2.75$ meV so that $\Delta = 0.02$ meV, consistent with the experimental upper bound. The cubic anisotropy also induces spin canting in a pattern identical to the tilting pattern of the TiO_6 octahedra in the *Pnma* structure. This is indeed the dominant component of the

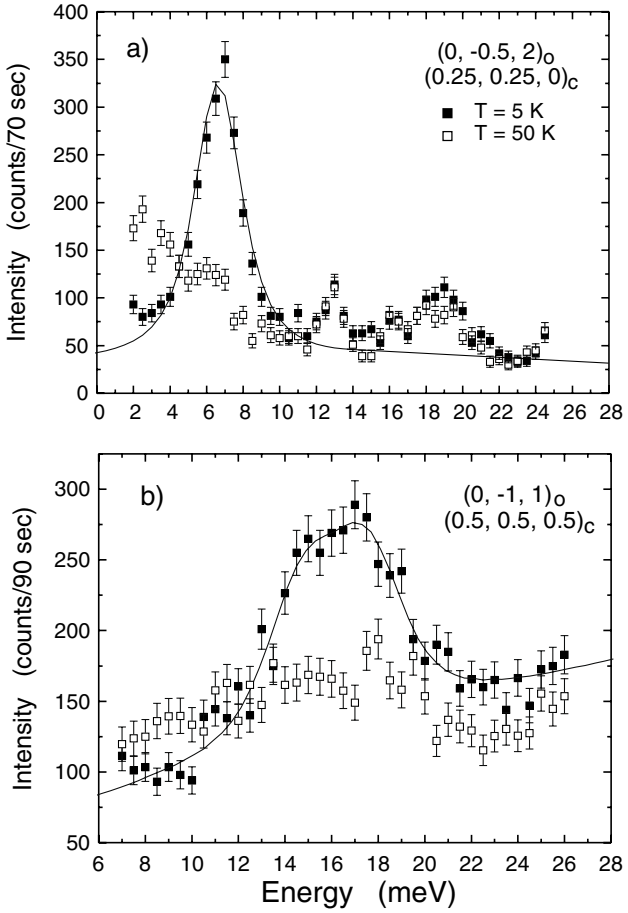

FIG. 2. Representative constant-$\mathbf{q}$ scans with (a) $\mathbf{q} = (\frac{1}{4}, \frac{1}{4}, 0)_c$ and (b) $\mathbf{q} = (\frac{1}{2}, \frac{1}{2}, \frac{1}{2})_c$ at 5 K ($< T_C$) and 50 K ($> T_C$). At 5 K both phonons and sharp magnons are present. The magnons become overdamped above T_C. The lines are results of a convolution of a magnon cross section with the spectrometer resolution function, as discussed in the text.

observed canting pattern (Fig. 1). An isotropic Heisenberg Hamiltonian with a small exchange anisotropy thus provides a good description of the magnetic ground state and dynamics.

While the neutron scattering data can be fitted by single, resolution limited profiles over most of the Brillouin zone [Fig. 2(a)], the profiles near the $(\frac{1}{2}, \frac{1}{2}, \frac{1}{2})_c$ point, where the magnon crosses an optical phonon branch at 19 meV, are broader than the instrumental resolution [Fig. 2(b)]. The same effective broadening was also observed in the spin-flip channel of a polarized-beam experiment. The best overall fit of the constant-Q scans near the zone boundary is obtained by two-peak profiles corresponding to two sharp but nondegenerate magnons [Fig. 2(b)]. The splitting of the magnon degeneracy probably originates from a hybridization of the magnon with the optical phonon. Magnon-phonon hybridization has been observed in other transition metal compounds and was attributed to a modulation of the crystal-field potential by the phonon [22]. However, as the two peaks are not completely resolved, other origins (such as a finite magnon lifetime) cannot be ruled out entirely at present.

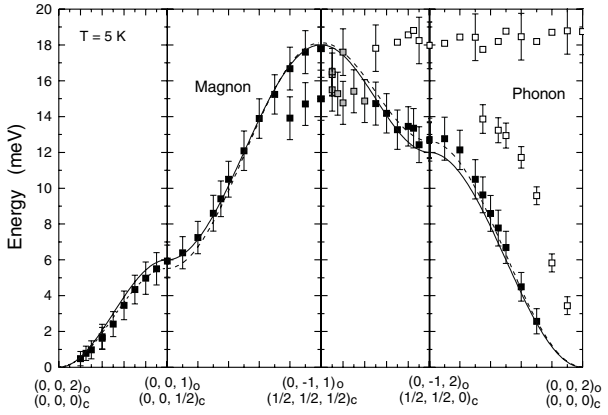

FIG. 3. Spin wave dispersion relations at $T = 5$ K. The solid symbols refer to magnetic excitations, whereas the open symbols can be identified as phonons. The grey points were extracted from scans at low temperatures, without a corresponding scan above T_C, so that an unambiguous identification is not yet possible. The solid line is the magnon dispersion relation derived from an isotropic Heisenberg model. The dashed line is the same model augmented by a spin anisotropy as discussed in the text.

Leaving these subtleties aside, we now discuss the overall features of the magnon spectrum in terms of the orbitally ordered state predicted by band structure calculations [5,6] and reported to be consistent with NMR [23] and neutron [18] form factor data. In this state, the d electron occupies the following orbitals on the four inequivalent Ti sites of the *Pnma* structure [5,6]:

$$|\psi\rangle_{1,3} = c_1|d_{yz}\rangle \pm c_2|d_{xy}\rangle,$$
$$|\psi\rangle_{2,4} = c_1|d_{xz}\rangle \pm c_2|d_{xy}\rangle. \quad (2)$$

Using the superexchange Hamiltonian given in Ref. [10] and the above wave functions, the expectation values of the c axis and in-plane exchange couplings are

$$J_c = J_{\mathrm{SE}}[(r_1 + r_2 r_3)(1 - n_{xy}) - (r_1 - r_2)](1 - n_{xy})/2,$$
$$J_{ab} = J_{\mathrm{SE}}[(r_1 + r_2 r_3)n_{xy}^2 - (r_1 - r_2)(1 + n_{xy})/2]/2. \quad (3)$$

Here $J_{\mathrm{SE}} = 4t^2/U$ (where t stands for the Ti-Ti hopping parameter and the parameter U for the Coulomb repulsion on the same t_{2g} orbital) represents the overall superexchange energy scale, and $n_{xy} = c_2^2$ is the fraction of the d_{xy} orbital controlling the orbital state. The coefficients $r_1 = 1/(1 - 3\eta)$, $r_2 = 1/(1 - \eta)$, and $r_3 = 1/(1 + 2\eta)$ originate from the Hund's rule splitting of the excited t_{2g}^2 multiplet by $\eta = J_H/U$. The parameters n_{xy} and η control the exchange couplings along the different axes and their ratio, as shown in Fig. 4.

In principle, one may obtain isotropic exchange parameters (that is, $J_c = J_{ab}$) of ferromagnetic sign [24] by using an orbital state with $n_{xy} \sim 0.6$ (close to the value reported in Ref. [18]). However, this requires a large, unrealistic value of the Hund coupling. For representative

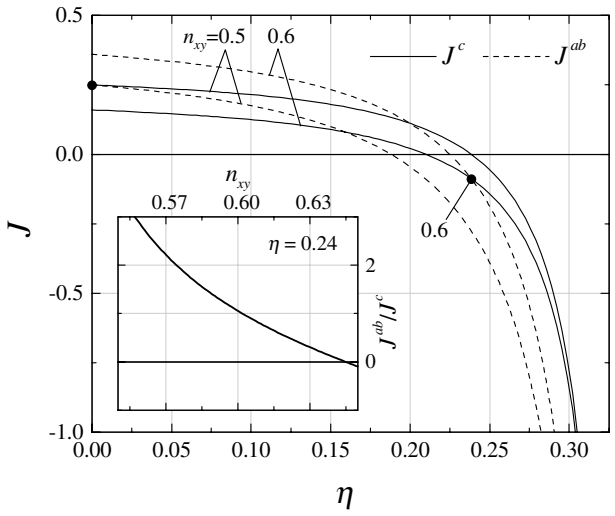

FIG. 4. Exchange constants (in units of J_{SE}) as a function of the Hund coupling η for different values of the parameter n_{xy} characterizing the orbital state. The inset shows the ratio of in-plane and out-of-plane exchange couplings for fixed η as a function of n_{xy}.

values of $J_H \sim 0.64\,\text{eV}$ and $U - \frac{20}{9}J_H \sim 4\,\text{eV}$ [5], one can estimate $\eta \sim 0.12$ which is inconsistent with isotropic, ferromagnetic exchange parameters (Fig. 4). Moreover, an unphysical fine tuning of the orbital state is required to obtain a spin Hamiltonian of cubic symmetry. Because of the high sensitivity of the spin interactions to the orbital state, even a small ($\sim 5\%$) change of n_{xy} leads to a strong spatial anisotropy of the coupling constants and may even reverse their relative sign (inset in Fig. 4).

An explanation of the small spin wave gap $\Delta \leq 0.3\,\text{meV}$ presents a further serious difficulty for the conventional Goodenough-Kanamori picture. The TiO_6 octahedra of $YTiO_3$ are elongated, leaving four almost equal Ti-O bonds [4,14,15]. To a first approximation, the crystal-field ground state should therefore be a quadruplet with substantial unquenched orbital angular momentum and a large magnon gap. Using the wave functions of Eq. (2) with parameters that result in $J_c = J_{ab} \sim -0.1 J_{SE}$, we have obtained a quantitative estimate of $\Delta \simeq J_{SE}(\lambda/D)^2$ for the gap due to the symmetric exchange anisotropy, where $\lambda \sim 15$–$20\,\text{meV}$ is the spin-orbit coupling constant and D is the crystal-field splitting of the two lowest-lying Kramers doublets. In addition, the Dzyaloshinskii-Moriya interaction cants the spins by an angle $\phi \simeq (J_{SE}/3|J|)(\lambda/D)$ away from the c axis and further increases the gap by $|J|\phi^2$. To be consistent with the experimentally determined canting angle and upper bound for the gap, D must be at least 200 meV, which is hard to reconcile with the tetragonal crystal-field environment of the Ti^{3+} ion.

These considerations imply the need to go beyond the standard Goodenough-Kanamori approach in order to arrive at a theoretical description of the nearly isotropic magnon spectrum of $YTiO_3$. While the experimental situation [18,23] precludes an orbitally disordered state such as the one proposed for $LaTiO_3$ [9,10], quantum zero-point fluctuations in the orbital sector naturally lead to magnon spectra with diminished spatial and spin anisotropies even if orbital order is not entirely obliterated [25].

In summary, we have shown that the magnon dispersions of $YTiO_3$ are an extremely sensitive gauge of the orbital state. The measured dispersions are inconsistent with the orbital states thus far proposed and point to the central importance of orbital zero-point fluctuations, an interesting subject of future research.

[1] For a recent review, see Y. Tokura and N. Nagaosa, Science **288**, 462 (2000).
[2] See, e.g., J.W. Lynn *et al.*, Phys. Rev. Lett. **76**, 4046 (1996); F. Moussa *et al.*, Phys. Rev. B **54**, 15 149 (1996); K. Hirota *et al.*, J. Phys. Soc. Jpn. **65**, 3736 (1996).
[3] E. Saitoh *et al.*, Nature (London) **410**, 180 (2001).
[4] D. A. MacLean, H. N. Ng, and J. E. Greedan, J. Solid State Chem. **30**, 35 (1979).
[5] T. Mizokawa and A. Fujimori, Phys. Rev. B **51**, 12 880 (1995); **54**, 5368 (1996); T. Mizokawa, D. I. Khomskii, and G. A. Sawatzky, *ibid.* **60**, 7309 (1999).
[6] H. Sawada and K. Terakura, Phys. Rev. B **58**, 6831 (1998).
[7] B. Keimer *et al.*, Phys. Rev. Lett. **85**, 3946 (2000).
[8] M. Mochizuki and M. Imada, J. Phys. Soc. Jpn. **70**, 2872 (2001).
[9] G. Khaliullin and S. Maekawa, Phys. Rev. Lett. **85**, 3950 (2000).
[10] G. Khaliullin, Phys. Rev. B **64**, 212405 (2001).
[11] Y. Taguchi, Y. Tokura, T. Arima, and F. Inaba, Phys. Rev. B **48**, 511 (1993).
[12] Y. Okimoto, T. Katsufuji, Y. Okada, T. Arima, and Y. Tokura, Phys. Rev. B **51**, 9581 (1995).
[13] D. A. McLean, K. Seto, and J. E. Greedan, J. Solid State Chem. **40**, 241 (1981).
[14] C. Ulrich and M. Reehuis (unpublished).
[15] V. G. Zubkov, I. F. Berger, A. M. Artamonova, and G. V. Bazuev, Sov. Phys. Crystallogr. **29**, 296 (1984).
[16] E. F. Bertaut, Acta Crystallogr. Sect. A **A24**, 217 (1968).
[17] As our data agree very well with an analysis based on spin canting alone, we have not considered effects arising from a possible alternation of the magnetic form factor due to orbital order, as discussed in Ref. [18].
[18] J. Akimitsu *et al.*, J. Phys. Soc. Jpn. **70**, 3475 (2001).
[19] M. Tsubota *et al.*, Physica (Amsterdam) **281B&282B**, 622 (2000).
[20] J. Kulda, program RESTRAX (private communication).
[21] G. S. Rushbrooke *et al.* in *Phase Transitions and Critical Phenomena*, edited by C. Domb and M. S. Green (Academic, New York, 1974).
[22] See, e.g., S. W. Lovesey, J. Phys. C **5**, 2769 (1972).
[23] M. Itoh, M. Tsuchiya, H. Tanaka, and K. Motoya, J. Phys. Soc. Jpn. **68**, 2783 (1999).
[24] S. Ishihara, T. Hatakeyama, and S. Maekawa, Phys. Rev. B **65**, 064442 (2002).
[25] G. Khaliullin and S. Okamoto, preceding Letter, Phys. Rev. Lett. **89**, 167201 (2002).